Supporting Online Information for:

Equilibrium and Kinetic Behavior of $Fe(CN)_6^{3-/4-}$ and Cytochrome *c* in Direct Electrochemistry Using a Film Electrode Thin-Layer Transmission Cell.

Yingrui Dai, Yi Zheng, Greg M. Swain and Denis A. Proshlyakov

Design of the Thin-Layer Spectroelectrochemical Cell.

When a metal grid is used as the working electrode, a solid non-conductive window (fused silica, Si etc.) is used in lieu of a film electrode. A thin layer of metal (50 Å Ti base, 200 Å Au coat) is deposited onto this window in all areas except for the center (9 mm dia.). The outer part of the metal grid is compressed between the spacer and metal-coated area of the window providing conductivity while the central part of the grid is loosely located inside the cavity.

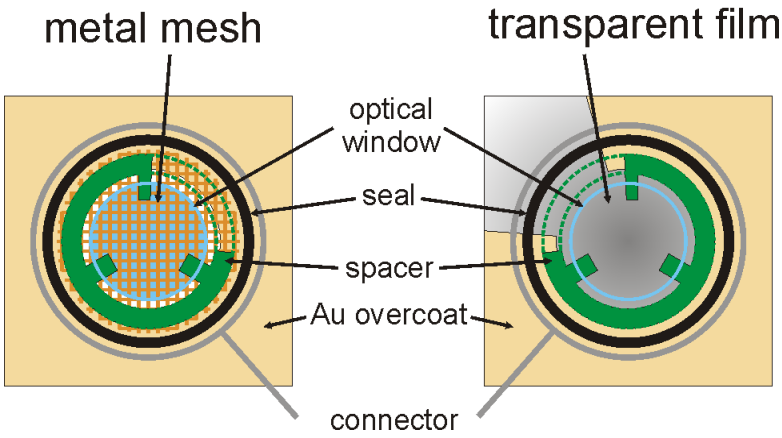

Figure S1 Schematic diagram of electrochemical cavity with metal mesh and transparent film working electrodes. Inherently conductive solid electrodes, such as glassy carbon, do not require Au overcoat.

The apparent thickness, *l*, of the cell with area *A* calculated from the faradaic charge for $Fe(CN)_6^{4-}$ (C^* = 1 mM) at scan rates ≤ 5mV was 58, 19, and 10 μm for 75, 25, and 7.5 μm spacers, respectively ($Q = n\,F\,A\,l\,C^*$). While calculated values for both the 25 and 75 μm layers were ~75% of the theoretical values, based on the geometric parameters of the cell, the 7.5 μm spacer yielded an effective thickness 133% of the design value in agreement with larger i_N and Q_N observed for this spacer. On the other hand, layer thickness determined from optical absorption measurements of

met-Mb (ε_{408}=188 $mM^{-1}cm^{-1}$) was in a good agreement with the theoretical values for all three spacers (60, 18 and 6 μm, respectively) indicating that the discrepancy in the electrochemical response with 7.5 μm spacer originates outside of the geometrically defined cell cavity.

We found that the 6 mm clear transmission aperture and the use of electrolyte capillary around the cell perimeter provide an optimum balance with the overall ohmic resistance. A variable spacer physically defines thickness of the layer and limits the diameter of the electrochemical chamber (Fig. 1), yielding predictable and reproducible response with well-defined thermodynamic (Fig. 2) and kinetic (Fig. 3) parameters. A larger diameter cell (19 mm) exhibited significantly slower and kinetically more heterogeneous response due to faster electrolysis on the perimeter of the layer with corresponding potential drop along the radial coordinate.

Electrode Materials. The glassy carbon electrode (Tokai, GC-20) was prepared by polishing to a mirror-like finish with successively smaller grades of alumina powder slurried in ultrapure water (1.0, 0.3, and 0.05 μm). The polishing was carried out by hand on individual felt polishing pads. After each polishing step, the electrode was thoroughly rinsed with ultrapure water and then ultrasonically cleaned in the same medium for 20 min to remove polishing debris and clean the surface. The gold minigrid electrode (Precision EForming, MG44, 55% transmission) was modified prior to each use by oxidizing in a freshly prepared, concentrated H_2SO_4:30% H_2O_2 (3:1 v/v) solution for 30 min followed by incubation in 2 mM cysteamine for 2 h.

An optically transparent boron-doped diamond thin film was deposited on quartz using a gas mixture consisting of 0.5% CH_4 in H_2 with 10 ppm B_2H_6 added for boron doping with a total gas flow of 100 sccm. Growth conditions were as described previously.[1, 2] A 1 h growth at ~650 ^oC yielded film with an electrical resistivity of ~0.026 Ω-cm and an optical transparency of 45-60% between 300 and 800 nm. The film was

soaked for 20 min in distilled isopropanol (stored over activated carbon) to clean the surface prior to use. To reduce the ohmic resistance in the measurement, a metallic layer (50 Å Ti, 200 Å Au) was deposited on the perimeter of the film not in contact with the electrolyte solution.

Anaerobic measurements. To eliminate entrapment of air bubbles in anaerobic measurements the cell was first fully assembled while submerged in aerobic deionized water. Assembled cell was flushed with high flow of anaerobic supporting electrolyte (5-10 ml) while venting sample discharge port and similar counter electrode ports (latter not shown in Fig. 1). Electrolyte solution was optionally supplemented with ~1 mM $Na_2S_2O_4$ which decomposed spontaneously within an hour or immediately upon application of positive potential as monitored at 350 nm. Following the flush, a small volume of sample (50-150 μl) was loaded into electrochemical cavity using microsyringe while extra ports were plugged. Hydrodynamic resistance of the capillary required a larger volume of sample for 7.5-12 μm spacers than for 50-75 μm spacers as observed following optical transmission changes.

Resistance of the cell to leaks of atmospheric oxygen was tested using deoxy-myoglobin as a sensitive probe.[3-5] Fully reversible optical changes were observed for $Mb^{+3} + e^- \leftrightarrow Mb^{+2}$ upon repetitive potential steps under intermittent optical sampling. Under continuous illumination conditions the reversible response shown in Figs. S2 was observed only when the far- to mid-UV spectral region of the probe light was blocked using an optical filter ($\lambda > 320$ nm). A well-defined isosbestic point (419.5 nm) observed in this case showed that no other processes were taking place under these conditions. Presence of oxygen in the sample would manifest itself by characteristic shift of the Soret absorption band from 434 to 419 nm upon formation of Fe^{2+}-O_2 oxy complex, particularly in a thin-layer configuration. No such changes were observed in the sample incubated in the dark overnight in the absence of applied potential providing supporting tight control over the gas phase in the cell.

Upon exposure of Mb to a full-spectrum UV probe light ($\lambda > 190$ nm) redox-difference optical changes were no longer reversible: the amplitude and the rate of optical changes rapidly diminished over time with the concurrent increase in the optical

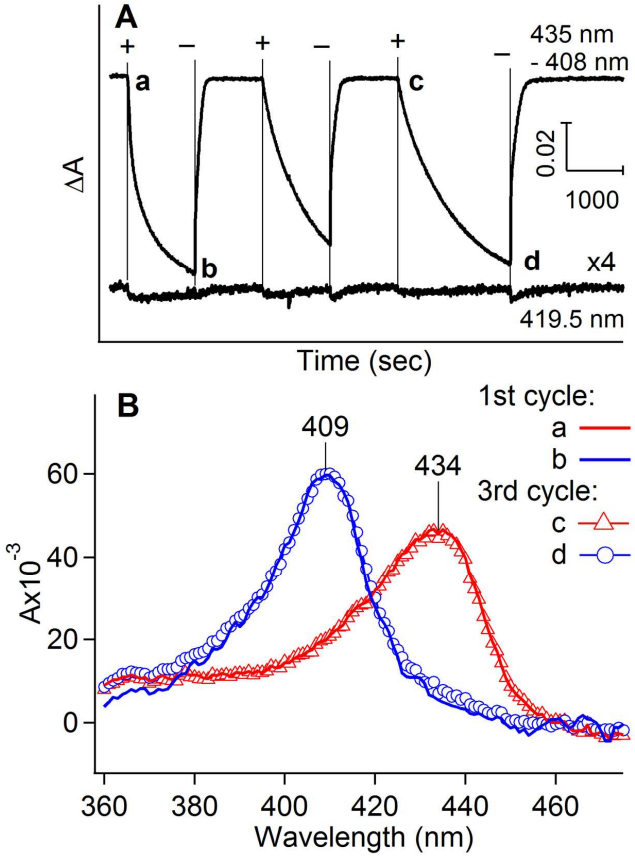

Figure S2 Absolute optical absorption spectra observed upon repetitive potential steps in anaerobic myoglobin. (A) Changes in the amplitude of the absorption difference between deoxy- and met-Mb (435 - 408 nm) and their isosbestic point (419.5 nm) upon potential steps between -0.7 V and +0.4 V obtained with a long-pass UV filter ($\lambda > 320$ nm) in the sample beam. (B) Positive (blue) and negative (red) potential spectra observed in the first and third redox cycles were essentially identical. Observed absorption maxima were characteristic of deoxy- and met-Mb. Data were recorded with Au-MG working electrode and 75 μm spacer. Sample: 0.05 mM anaerobic deoxy-myoglobin in 100 mM sodium phosphate buffer (pH 7), 0.1 M KCl.

absorption at the isosbestic point. Similar changes were also observed in the absence of applied potential. This behavior was attributed to photochemical oxidation of aromatic residues leading to its structural damage, although details of this mechanism extend beyond the scope of the present study.

Deviations from the ideal thin layer behavior. At higher scan rates and analyte concentration with the 75 μm spacer, we observed some distortion of CV peaks and increased ΔE_p, which can be attributed to a combination of ohmic resistance and the thickness of the layer approaching the $\sqrt{2Dt}$ term, where D is the diffusion coefficient of the analyte and t is the time scale of the measurement. The unchanging ΔE_p with increasing analyte concentration under other conditions demonstrates that relatively sluggish electron-transfer kinetics at the electrode surface is the main cause of the nonzero ΔE_p, not ohmic effects.

The second deviation occurred at minimal layer thickness where Q, i_p and ΔE_p were larger than predicted from the cell geometry. This behavior can be rationalized by considering the diffusion of analyte in the electrochemical capillary (EC, Fig. 1) toward the electrode similar to the analyte in the thin layer. The maximal depth of such diffusion, or the diffusion limit, is determined only by the allowed time (DL=$\sqrt{2Dt}$ in Fig. 1). For thicker layers (75 μm), which are comparable with the diffusion limit, the volume of EC between DL and TL is negligible comparing to the volume of TL over entire electrode. As the TL decreases for the 25 and 7.5 μm spacers and DL remains unchanged, the relative contribution of electroactive volume in EC increases to a noticeable level. Extrapolation of total charge to zero layer thickness provides an estimate of electroactive volume in EC at ~0.2 μL with the maximal contribution ~1/3 of total electrochemical response at 7.5 μm layer.

REFERENCES

1. J. Stotter, J. Zak, Z. Behler, Y. Show and G. M. Swain, *Anal. Chem.*, 2002, **74**, 5924-5930.

2. J. Stotter, Y. Show, S. Wang and G. Swain, *Chem. of Mater.*, 2005, **17**, 4880-4888.

3. R. Hill, *P Roy Soc Lond B Bio*, 1936, **120**, 472-483.

4. J. J. Kelly, K. A. Kelly, S. A. Hartley and C. H. Barlow, *Appl Spectrosc*, 1991, **45**, 1177-1182.

5. P. K. Grzyska, R. P. Hausinger and D. A. Proshlyakov, *Anal Biochem*, 2010, **399**, 64-71.

Table S1 Average peak potentials of $Fe(CN)_6^{3-/4-}$ observed during cyclic voltammetry in the thin layer cell.

		7 μm spacer		25 μm spacer		75 μm spacer	
C mM	scan rate mV/s	$E_{1/2}$ mV	ΔE_p mV	$E_{1/2}$ mV	ΔE_p mV	$E_{1/2}$ mV	ΔE_p mV
0.25	1	**286.6** ±4.0	**35.75** ±2.6	**287.0** ±4.7	**15.71** ±3.9	**284.1** ±4.9	**13.75** ±3.9
	2	**287.0** ±6.5	**34.40** ±10.1	**285.3** ±5.3	**20.00** ±2.2	**282.5** ±5.8	**21.50** ±1.9
	5	**286.2** ±3.8	**39.20** ±9.1	**285.5** ±4.2	**25.29** ±5.2	**283.3** ±5.7	**33.00** ±3.7
	10	**285.6** ±2.7	**44.80** ±9.1	**285.9** ±4.9	**29.00** ±8.2	**282.8** ±5.7	**45.00** ±5.6
	20	**286.0** ±2.6	**46.40** ±11.7	**284.6** ±5.3	**34.86** ±9.5	**282.9** ±5.0	**61.75** ±7.4
0.5	1	**287.1** ±4.4	**23.25** ±5.3	**285.0** ±4.6	**14.00** ±2.5	**281.9** ±4.1	**13.75** ±2.6
	2	**285.3** ±5.0	**28.00** ±6.2	**284.9** ±3.5	**16.57** ±1.5	**282.3** ±5.3	**18.50** ±1.9
	5	**285.3** ±4.6	**34.00** ±5.0	**285.1** ±4.5	**24.29** ±4.0	**281.4** ±5.6	**33.25** ±4.8
	10	**285.8** ±3.1	**41.50** ±7.6	**285.0** ±4.1	**31.14** ±6.9	**282.1** ±5.0	**49.75** ±6.7
	20	**284.5** ±3.8	**47.50** ±12.0	**284.0** ±4.3	**40.00** ±9.3	**280.9** ±5.1	**69.25** ±10.5
1	1	**284.8** ±3.5	**26.00** ±5.6	**285.0** ±3.6	**16.86** ±0.9	**281.8** ±4.2	**11.50** ±4.1
	2	**285.5** ±4.2	**27.00** ±4.8	**284.6** ±4.2	**18.29** ±2.7	**282.4** ±4.9	**19.75** ±7.2
	5	**285.6** ±3.9	**35.25** ±7.0	**284.7** ±4.5	**24.86** ±4.2	**280.9** ±4.9	**36.75** ±13.8
	10	**284.6** ±4.3	**47.25** ±10.2	**283.7** ±3.3	**34.86** ±7.3	**280.8** ±4.9	**55.50** ±19.2
	20	**284.4** ±2.5	**54.75** ±21.0	**283.7** ±3.9	**47.71** ±12.1	**280.6** ±4.3	**79.25** ±28.8

Average values for midpoint potential ($E_{½}$), peak separation (ΔE_p) and corresponding standard deviations were obtained for n≥3 measurements carried out on a glassy carbon working electrode in 1 M KCl as a supporting electrolyte.

Table S2 Average peak current observed for $Fe(CN)_6^{3-/4-}$ during cyclic voltammetry in the thin layer cell.

		7 μm spacer		25 μm spacer		75 μm spacer	
C mM	scan rate mV/s	i_p μA	i_a/i_c	i_p μA	i_a/i_c	i_p μA	i_a/i_c
0.25	1	**0.3** ±0.07	**0.94** ±0.08	**0.4** ±0.05	**1.03** ±0.06	**1.1** ±0.10	**0.98** ±0.04
	2	**0.5** ±0.09	**0.97** ±0.05	**0.8** ±0.09	**1.05** ±0.04	**2.1** ±0.20	**0.97** ±0.04
	5	**0.9** ±0.15	**0.97** ±0.03	**1.6** ±0.15	**0.98** ±0.05	**4.8** ±0.34	**0.96** ±0.03
	10	**1.4** ±0.24	**0.96** ±0.02	**2.8** ±0.27	**0.97** ±0.05	**8.3** ±0.56	**0.95** ±0.02
	20	**2.3** ±0.39	**0.99** ±0.03	**5.0** ±0.40	**0.95** ±0.04	**13.5** ±0.85	**0.94** ±0.01
0.5	1	**0.6** ±0.10	**1.00** ±0.05	**0.9** ±0.08	**1.04** ±0.04	**2.3** ±0.13	**0.99** ±0.02
	2	**1.0** ±0.18	**0.98** ±0.04	**1.5** ±0.14	**1.02** ±0.04	**4.4** ±0.25	**0.98** ±0.03
	5	**2.0** ±0.37	**0.99** ±0.02	**3.3** ±0.28	**1.00** ±0.03	**9.7** ±0.53	**0.96** ±0.02
	10	**3.3** ±0.64	**1.00** ±0.02	**5.7** ±0.51	**0.97** ±0.03	**17.0** ±0.93	**0.95** ±0.02
	20	**5.3** ±1.06	**0.99** ±0.03	**10.0** ±0.91	**0.97** ±0.03	**27.6** ±1.47	**0.94** ±0.01
1	1	**1.2** ±0.12	**1.02** ±0.05	**1.6** ±0.17	**1.04** ±0.03	**4.5** ±0.25	**1.00** ±0.01
	2	**2.0** ±0.20	**1.02** ±0.02	**2.8** ±0.30	**1.04** ±0.01	**8.5** ±0.43	**0.99** ±0.01
	5	**3.9** ±0.40	**1.00** ±0.01	**6.0** ±0.66	**1.00** ±0.01	**19.2** ±1.04	**0.97** ±0.01
	10	**6.5** ±0.77	**1.00** ±0.01	**10.5** ±1.18	**0.99** ±0.02	**33.8** ±2.18	**0.96** ±0.01
	20	**10.5** ±1.22	**1.00** ±0.01	**18.3** ±2.17	**0.98** ±0.02	**55.4** ±4.32	**0.95** ±0.01

Average values between anodic and cathodic peak currents ($i_p = \frac{1}{2}(i_c + i_a)$), their ratios ($i_a/i_c$), and corresponding standard deviations were obtained from the same data shown in table **S1**.

Table S3 Average faradaic charge observed for $Fe(CN)_6^{3-/4-}$ during cyclic voltammetry in the thin layer cell.

		7 μm spacer		25 μm spacer		75 μm spacer	
C mM	Scan rate mV/s	*Q* μC	Q_a/Q_c	*Q* μC	Q_a/Q_c	*Q* μC	Q_a/Q_c
0.25	1	**40.3** ±11.0	**0.97** ±0.06	**55.4** ±7.6	**1.07** ±0.08	**128.9** ±13.7	**1.01** ±0.03
	2	**32.0** ±6.9	**0.99** ±0.09	**49.6** ±7.2	**1.10** ±0.06	**123.8** ±13.7	**1.01** ±0.04
	5	**25.0** ±4.6	**0.97** ±0.08	**41.9** ±3.6	**1.02** ±0.06	**114.5** ±9.6	**1.01** ±0.02
	10	**20.0** ±3.8	**0.96** ±0.04	**35.7** ±4.1	**1.01** ±0.04	**106.4** ±8.1	**0.98** ±0.01
	20	**15.8** ±2.7	**1.00** ±0.05	**31.9** ±3.0	**0.98** ±0.04	**96.3** ±6.7	**0.98** ±0.01
0.5	1	**82.0** ±14.7	**1.00** ±0.08	**108.6** ±8.6	**1.06** ±0.08	**263.1** ±12.4	**1.04** ±0.02
	2	**68.9** ±11.8	**0.99** ±0.08	**94.9** ±7.4	**1.05** ±0.10	**249.0** ±15.0	**1.01** ±0.02
	5	**54.3** ±9.7	**0.99** ±0.07	**81.1** ±6.3	**1.03** ±0.03	**229.8** ±12.2	**1.01** ±0.02
	10	**45.4** ±8.5	**1.05** ±0.03	**70.6** ±5.0	**1.00** ±0.03	**216.3** ±10.2	**0.99** ±0.01
	20	**37.1** ±7.4	**1.01** ±0.05	**63.1** ±4.1	**0.99** ±0.02	**198.1** ±8.4	**0.99** ±0.01
1	1	**155.2** ±13.3	**1.02** ±0.08	**199.1** ±18.2	**1.04** ±0.06	**507.9** ±32.1	**1.02** ±0.01
	2	**139.3** ±14.3	**1.03** ±0.06	**173.7** ±17.0	**1.08** ±0.03	**481.0** ±27.2	**1.02** ±0.01
	5	**107.0** ±9.5	**1.02** ±0.00	**147.9** ±14.5	**1.02** ±0.01	**448.0** ±20.7	**1.00** ±0.01
	10	**89.3** ±10.9	**1.03** ±0.02	**131.5** ±12.6	**1.01** ±0.01	**425.8** ±17.9	**1.00** ±0.01
	20	**76.4** ±9.5	**1.03** ±0.02	**117.4** ±10.1	**1.00** ±0.02	**396.6** ±15.8	**0.99** ±0.01

Average values between anodic and cathodic faradaic charges ($Q = \frac{1}{2}(Q_c + Q_a)$), their ratios ($Q_a/Q_c$), and corresponding standard deviations were obtained from the same data shown in table **S1**.